EC
Journals.ASM.org

Rsr1 Focuses Cdc42 Activity at Hyphal Tips and Promotes Maintenance of Hyphal Development in *Candida albicans*

Rebecca Pulver,[b] Timothy Heisel,[a] Sara Gonia,[a] Robert Robins,[a] Jennifer Norton,[a]* Paula Haynes,[a]* Cheryl A. Gale[a,b]

Departments of Pediatrics[a] and Genetics, Cell Biology and Development,[b] University of Minnesota, Minneapolis, Minnesota, USA

The extremely elongated morphology of fungal hyphae is dependent on the cell's ability to assemble and maintain polarized growth machinery over multiple cell cycles. The different morphologies of the fungus *Candida albicans* make it an excellent model organism in which to study the spatiotemporal requirements for constitutive polarized growth and the generation of different cell shapes. In *C. albicans*, deletion of the landmark protein Rsr1 causes defects in morphogenesis that are not predicted from study of the orthologous protein in the related yeast *Saccharomyces cerevisiae*, thus suggesting that Rsr1 has expanded functions during polarized growth in *C. albicans*. Here, we show that Rsr1 activity localizes to hyphal tips by the differential localization of the Rsr1 GTPase-activating protein (GAP), Bud2, and guanine nucleotide exchange factor (GEF), Bud5. In addition, we find that Rsr1 is needed to maintain the focused localization of hyphal polarity structures and proteins, including Bem1, a marker of the active GTP-bound form of the Rho GTPase, Cdc42. Further, our results indicate that tip-localized Cdc42 clusters are associated with the cell's ability to express a hyphal transcriptional program and that the ability to generate a focused Cdc42 cluster in early hyphae (germ tubes) is needed to maintain hyphal morphogenesis over time. We propose that in *C. albicans*, Rsr1 "fine-tunes" the distribution of Cdc42 activity and that self-organizing (Rsr1-independent) mechanisms of polarized growth are not sufficient to generate narrow cell shapes or to provide feedback to the transcriptional program during hyphal morphogenesis.

Fungal hyphae are able to elongate over large distances and must allocate their cellular resources in order to maintain extremely polarized growth for extended periods of time. The multimorphic opportunistic fungal pathogen *Candida albicans* provides a useful model system in which to investigate the basic cell biological and genetic mechanisms that generate highly polarized cell shapes and the requirements for hyphal development. *C. albicans* has a true hyphal growth form, as well as pseudohyphal and yeast forms, and reversibly switches between these morphologies depending on environmental conditions (reviewed in reference 1). Yeast cells are ellipsoid, propagate by budding, and undergo cytokinesis and cell separation. Pseudohyphae are more elongated than yeast cells and do not undergo cell separation, resulting in the formation of chains of elongated daughter cells. Hyphae, in contrast, are extremely elongated, narrow cells, and their development can be thought of as two continuous stages, early growth and development of germ tubes (GTs) followed by the development and maintenance of mature hyphae. GTs enter the maintenance phase of polarized growth, transitioning to mature hyphae, after the formation of the first septum, a specialized structure that delimits cellular compartments. Whereas morphogenesis mechanisms in *C. albicans* yeast and pseudohyphae appear to follow those of the similar morphologies in *Saccharomyces cerevisiae*, it is unclear if, or how, these mechanisms are modified to enable the development of the highly elongated hyphal form.

Localized activation of Rho GTPases underlies actin-based cell polarization and morphogenesis in eukaryotic cell systems (reviewed in reference 2). In *C. albicans*, the role of the essential Rho GTPase Cdc42 is thought to impact hyphal development in *C. albicans* in at least two ways. First, the amount of Cdc42 affects the morphogenesis program at the transcriptional level. Strains expressing reduced levels of Cdc42 have decreased expression of hyphal-specific genes (HSGs), some of which are important for production of hyphal-morphogenesis characteristics and hyphal-associated virulence factors (3). Second, Cdc42 activates and localizes proteins needed for polarized growth. Decreasing cellular levels of Cdc42 result in both yeast and hyphae that have larger and rounder cell shapes indicative of a defect in polarized growth (3–5). Clusters of Cdc42 localize at incipient growth sites periodically during bud initiation in yeast, while during *C. albicans* hyphal morphogenesis, Cdc42 clusters localize constitutively to hyphal tips in an F-actin-dependent manner (6). In yeast cells, growth sites are dictated by internal landmarks, such as the Ras-like GTPase Rsr1 (7). In hyphae, although germ tube emergence sites can be directed by external electrical cues (8), it is unclear if an internal landmark mechanism directs germ tube emergence sites under noncued conditions (9, 10). In the end, effectors of Cdc42 are recruited to these growth initiation sites and direct the polarization of the actin cytoskeleton to ultimately target secretion to the daughter cell apex.

C. albicans hyphae contain a tip-localized polarity structure not found in yeast and pseudohyphae called a Spitzenkörper (Spk). The Spk is a developmental hallmark of hyphal growth that is observed in the majority of cultured filamentous fungi and is required for hyphal cell shape (reviewed in reference 11). Forma-

Received 2 November 2012 **Accepted** 28 November 2012

Published ahead of print 7 December 2012

Address correspondence to Cheryl A. Gale, galex012@umn.edu.

* Present address: Jennifer Norton, University of Arizona College of Medicine, Department of Cellular and Molecular Medicine, Tucson, Arizona, USA; Paula Haynes, Brandeis University, Waltham, Massachusetts, USA.

Supplemental material for this article may be found at http://dx.doi.org/10.1128/EC.00294-12.

doi:10.1128/EC.00294-12

tion and maintenance of the Spk require that polarized actin cables, a downstream result of localized Cdc42 activity, be directed toward hyphal tips (12). Spks are composed of accumulations of vesicles and proteins and, as a unit, act as reservoirs to supply extending tips with the components needed to maintain continuous hyphal growth (13, 14). Although it is clear that polarity factors such as the Spk need to be maintained constitutively at cell apices for hyphal growth to continue, the mechanism by which this occurs is not understood.

Proposed mechanisms for polarity establishment and maintenance have been derived from the results of studies using *S. cerevisiae*. These studies focused on how cortical Cdc42 clusters with an optimized distribution are formed and stabilized to promote bud initiation and early bud growth. These mechanisms require that activated Cdc42 be continually supplied to sites of growth, while its lateral diffusion at the membrane is simultaneously restricted in order to generate the discrete focus of Cdc42 activity needed for growth initiation (reviewed in reference 15). In addition, the size of the Cdc42 cluster has been shown to influence the shape of the growing daughter cell (16). This optimal Cdc42 cluster, or "window," is proposed to be achieved by a combination of processes, including positive-feedback mechanisms that increase Cdc42 activity at the growth site, membrane diffusion, local limitation of substrates (e.g., Cdc42 and its regulators and/or effectors), and active removal of Cdc42 from the membrane adjacent to the site of growth (16–18). It remains unknown how, and if, similar Cdc42 regulatory mechanisms are employed to regulate cell shape and maintain continuous polarization during *C. albicans* hyphal morphogenesis.

We previously reported that *C. albicans* strains lacking the landmark GTPase Rsr1 have defects in yeast and hyphal morphogenesis; *rsr1*Δ/Δ yeast cells are larger and rounder, and hyphae are wider, than those of wild-type (WT) control strains (7). These phenotypes are similar to those observed in *C. albicans* strains with reduced expression of Cdc42 (3) and were unexpected because the ortholog of Rsr1 in *S. cerevisiae* (ScRsr1), although interacting physically with Cdc42, is important for bud site selection, but not for polarized growth (19). Thus, we hypothesized that *C. albicans* Rsr1 (CaRsr1) has a role in polarized growth and morphogenesis beyond that of simply determining the location of Cdc42 activity.

In the current study, we aimed to understand how Rsr1 is involved in the assembly and/or maintenance of tip-localized polarity factors and how the localization features of these factors correlate with hyphal morphogenesis. Overall, our results are consistent with the idea that, in *C. albicans*, Rsr1 is needed for the efficient assembly of a focused Cdc42 cluster in GTs, which in turn is important for the continued maintenance of hyphal development.

MATERIALS AND METHODS

Media and growth conditions. Strains were grown on synthetic dextrose complete (SDC) (20) agar medium at 30°C, followed by transfer of a colony into SDC liquid medium at 30°C, and grown overnight to obtain stationary-phase yeast form cultures, unless otherwise noted. For all imaging experiments, hyphae were induced by growth of 25 μl of overnight yeast cultures in 1 ml of prewarmed (37°C) SDC medium plus 10% bovine serum. Uridine (80 μg/ml) was added to all media, except when selecting for uridine prototrophs during strain construction. Regulatable expression of genes from the *MET3* promoter was achieved by growth of strains in media lacking (expression) or containing (repression) methionine and cysteine, as previously described (21).

For quantitative fluorescence indexing and fluorescent fusion protein localization experiments in hyphae, 150 μl of diluted cells was placed onto poly-L-lysine (PLL)-coated slides and grown in humidified chambers at 37°C. For time-lapse microscopy, hyphae were grown on agarose pads with coverslips applied (except in FM4-64-staining experiments). Growth times were established relative to the completion of the first cell cycle, with 30 and 90 min (depending on the experiment) representing GTs (no septa had formed) and 3 h and 4 h representing mature hyphae (septa were present).

Strains and strain construction. The yeast strains used in this study are listed in Table 1. Fluorescent-protein fusions were constructed by PCR-mediated gene modification as previously described (26, 27), using the primers listed in Table S1 in the supplemental material. Constructions were verified by PCR using primers targeting sequences outside the sites of integration. In addition, expression of fluorescent proteins was evaluated by fluorescence microscopy and Western blotting, as described below.

Due to the lack of an available auxotrophy in the original *RSR1*-reintegrant control strain, it was necessary to reconstruct *rsr1*-null and -reintegrant strains in order to introduce *MLC1-YFP* and *BEM1-YFP* fusions into them. To do this, the two *RSR1* alleles were sequentially disrupted in *C. albicans* strain BWP17 by PCR-mediated gene modification using the *dpl200* sequence, as previously described (28), with primers 1460 and 1265 (see Table S1 in the supplemental material) and plasmid p1653 (28) as the DNA template. Disruption of both *RSR1* alleles in the resulting strain, CA12363, was verified by PCR using primer sequences located outside the sites of integration and by reverse transcription (RT)-PCR using primers targeting *RSR1* mRNA (data not shown). To construct *RSR1*-reintegrant control strains, disrupted and wild-type *RSR1* sequences were integrated into an *rsr1*::*dpl200* locus using linearized pMG2157 and pMG2128 to construct the control strains CA12431 (*rsr1*::*rsr1*/*rsr1*) and CA12430 (*RSR1*::*rsr1*/*rsr1*), respectively, as previously described (7, 8). Strain constructions were verified by PCR using primer sets that distinguished integration of the disrupted *rsr1* and full-length *RSR1* sequences into the promoter region of the deleted *rsr1* locus and confirmed by RT-PCR of *RSR1* mRNA (data not shown).

Western blotting. Five hundred microliters of yeast cell culture was harvested from overnight cultures, washed in water, inoculated into 10 ml of hypha-inducing medium, and grown at 37°C to obtain GTs and mature hyphae. The entire 10 ml of each hyphal culture was harvested, washed, and resuspended in 150 μl of 4% ULSB (20 mM Tris, pH 6.8, 10% glycerol, 0.005% bromophenol blue, 6 M urea, 4% SDS, and 20 mM dithiothreitol). Cell lysis and denaturation of proteins were achieved in one step by heating the resuspended cells in ULSB for 5 min at 100°C. The protein concentrations of the resulting lysates were determined spectrophotometrically (A_{280}) and diluted to equalize the concentrations of the samples. Protein samples were separated on SDS-polyacrylamide gels (12%) and then transferred to a polyvinylidene difluoride (PVDF) membrane, blocked for 30 min with 2% milk buffer (skim milk in TBST [20 mM Tris, pH 7.6, 137 mM NaCl, 0.1% Tween 20]), and incubated with the appropriate primary antibody (mouse anti-green fluorescent protein [α-GFP] [Roche, Indianapolis, IN; 1:2,000], rat-anti-Cdc42 [Santa Cruz Biotechnology, Santa Cruz, CA; 1:5,000], or rat anti-α-tubulin [Ab-Cam, Cambridge, MA; 1:5,000]) diluted in 0.2% milk buffer for 1 h. The blots were washed in TBST and incubated with the appropriate horseradish peroxidase-conjugated secondary antibody (goat α-mouse IgG [Santa Cruz Biotechnology, Santa Cruz, CA; 1:10,000], goat α-rat IgG [Santa Cruz Biotechnology, Santa Cruz, CA; 1:10,000], or goat α-rabbit IgG [Southern Biotech, Birmingham, AL; 1:10,000]) diluted in 0.2% milk buffer for 1 h. The blots were washed again in TBST and developed using the Supersignal Fempto Chemiluminescent reagent (Pierce, Rockford, IL). The amount of protein detected (signal intensity) was quantified using an Alpha-Innotech (San Leandro, CA) Chemi-Imager and Image-Quant image analysis software (GE Healthcare Biosciences, Pittsburgh, PA). The background-subtracted intensity was obtained using Image J (29), and the ratio of the amount of the protein of interest to that of tubulin was calculated.

TABLE 1 Yeast strains used in this study

C. albicans strain	Relevant genotype	Source
BWP17	*ura3*::λ*imm434/ura3*::λ*imm434 his1*::*hisG/his1*::*hisG arg4*::*hisG/arg4*::*hisG*	22
JB6284/9955	(BWP17) *his1*::*hisG/hisG*::*his1*::*HIS1 arg4*::*hisG/ARG4-URA3*::*arg4*::*hisG*	23
JB7783	(BWP17) *his1*::*hisG/hisG*::*his1*::*HIS1 arg4*::*hisG/ARG4*::*arg4*::*hisG*	24
CA8832	(BWP17) *rsr1*::*ARG4/rsr1*::*HIS1*	7
CA8880	(BWP17) *rsr1*::*ARG4/rsr1*::*HIS1 arg4*::*hisG/ARG4-URA3*::*arg4*::*hisG*	7
MG7139	(BWP17) *MLC1/MLC1-YFP-URA3*	12
CA9151	(BWP17) *rsr1*::*ARG4/rsr1*::*HIS1 MLC1/MLC1-YFP-URA3*	This study
CA10055	(BWP17) *URA3*-P_{MET3}-*YFP*::*BUD2/BUD2*	This study
CA12363	(BWP17) *rsr1*::*dpl200/rsr1*::*dpl200*	This study
CA12388	(BWP17) *rsr1*::*dpl200/rsr1*::*dpl200 MLC1/MLC1-YFP-HIS1*	This study
CA12430	(BWP17) *rsr1*::*dpl200/rsr1*::*dpl200 MLC1/MLC1-YFP-HIS1 pURA3-RSR1*::*rsr1*::*dpl200*	This study
CA12431	(BWP17) *rsr1*::*dpl200/rsr1*::*dpl200 MLC1/MLC1-YFP-HIS1 rsr1*::*dpl200*::*rsr1:URA3*	This study
CA12343	(BWP17) *URA3*-P_{MET3}-*YFP*::*BUD5/BUD5*	This study
CA12345	(BWP17) *URA3*-P_{MET3}-*YFP*::*RSR1/RSR1*	This study
CA9215	(BWP17) *rsr1*::*ARG4/*p*URA3-RSR1*::*rsr1*::*HIS1*	7
CA9339	(BWP17) *rsr1*::*ARG4/*p*URA3-rsr1*::*rsr1*::*HIS1*	8
CA12168	(JB7783) *BEM1/BEM1-YFP-URA3*	This study
CA12183	(BWP17) *rsr1*::*ARG4/rsr1*::*HIS1 BEM1/BEM1-YFP-URA3*	This study
CA12567	(BWP17) *rsr1*::*dpl200/rsr1*::*dpl200* p*URA3-RSR1*::*rsr1*::*dpl200*	This study
CA12570	(BWP17) *rsr1*::*dpl200/rsr1*::*dpl200* p*URA3-rsr1*::*rsr1*::*dpl200*	This study
CA12595	(BWP17) *rsr1*::*dpl200/rsr1*::*dpl200* p*URA3-RSR1*::*rsr1*::*dpl200 BEM1/BEM1-YFP-HIS1*	This study
CA12598	(BWP17) *rsr1*::*dpl200/rsr1*::*dpl200* p*URA3-rsr1*::*rsr1*::*dpl200*	This study
CA10271	*BEM1/BEM1-YFP-HIS1* (BWP17) *rga2*::*HIS1/rga2*::*ARG4 bem3*::*ura3*(5′Δ)/*bem3*::*ura3*(5′Δ)	25
CA10755	(BWP17) *rga2*::*HIS1/rga2*::*ARG4 bem3*::*ura3*(5′Δ)/*bem3*::*ura3*(5′Δ) *rsr1*::*dpl200/rsr1*::*dpl200*	This study
CA12188	(BWP17) *rga2*::*HIS1/rga2*::*ARG4 bem3*::*ura3*(5′Δ)/*bem3*::*ura3*(5′Δ) *arg4*::*hisG/ARG4-URA3*::*arg4*::*hisG*	This study
CA12191	(BWP17) *rga2*::*HIS1/rga2*::*ARG4 bem3*::*ura3*(5′Δ)/*bem3*::*ura3*(5′Δ) *rsr1*::*dpl200/rsr1*::*dpl200 arg4*::*hisG/ARG4-URA3*::*arg4*::*hisG*	This study
CA12172	(BWP17) *rga2*::*HIS1/rga2*::*ARG4 bem3*::*ura3*(5′Δ)/*bem3*::*ura3*(5′Δ) *BEM1/BEM1-YFP:HIS1*	This study
CA12173	(BWP17) *rga2*::*HIS1/rga2*::*ARG4 bem3*::*ura3*(5′Δ)/*bem3*::*ura3*(5′Δ) *rsr1*::*dpl200/rsr1*::*dpl200 BEM1/BEM1-YFP:HIS1*	This study

Image acquisition and processing. All images (except those obtained during fluorescence recovery after photobleaching [FRAP]) were collected on a Nikon E600 microscope equipped with 60×/1.4-numerical-aperture (NA) and 100×/1.4-NA objectives, FCS2 objective heaters (Bioptechs, Butler, PA), and epifluorescence. MetaMorph version 6.3r7 (Molecular Devices LLC, Sunnyvale, CA) was used for acquisition and processing of all images. Differential interference contrast (DIC) images were collected in conjunction with fluorescent images in all cases, using 50-ms exposures. Final representative images for publication were adjusted for brightness and contrast, cropped, and resized as a group for each set of experiments using Photoshop CS3 (Adobe Systems Inc., San Jose, CA).

(i) Imaging YFP-Rsr1, YFP-Bud5, and YFP-Bud2 localization. Images of yellow fluorescent protein (YFP)-tagged versions of Rsr1 (exposure, 800 ms; range, 10; step size, 2; 5 steps), Bud5 (exposure, 800 ms; range, 10; step size, 5; 3 steps), and Bud2 (exposure, 600 ms; range, 10; step size, 5; 3 steps) were collected using a 60× objective. The resultant stacked images were merged using summation, and the intensities were adjusted in MetaMorph before being exported to, and scaled together in, Photoshop.

(ii) Imaging FM4-64-stained hyphae. To obtain images used in determining fluorescence indices, hyphae were stained with 165 mM FM4-64 for 10 min (30). Excess medium and stain were aspirated, and cells were imaged as soon as technically feasible using the 60× objective. Approximately 10 images were captured for each strain using identical acquisition settings (10-ms exposure; shutter open between steps; 2-by-2 binning; range, 10; step size, 5; 3 steps), and replicate experiments were carried out on three separate days. To assess for differences in FM4-64 uptake between mutant and control strains, a mixed subculture of WT cells expressing Nop1-GFP and *rsr1*Δ/Δ cells was placed on PLL-coated slides and grown in hypha-inducing medium to obtain either GTs or mature hyphae. Cells were stained as before with FM4-64, coverslips were sealed to the slides with stopcock grease, and the cells were imaged using a 60× objective heated to 37°C. A GFP image (50-ms exposure time) was captured after completion of the time-lapse acquisition to identify WT (GFP-expressing) hyphae during quantification. FM4-64 localization was imaged over 1 h at 10-min intervals using acquisition settings identical to those stated above.

(iii) Imaging Mlc1-YFP and Bem1-YFP localization in hyphae. All images were acquired using a 60× objective heated to 37°C with the following acquisition settings: for myosin light chain 1 (Mlc1)-YFP, 500-ms exposure, shutter closed between steps, 2-by-2 binning, step size of 5, 3 steps; for Bem1-YFP, acquisition settings were the same, except that 300-ms exposure times were used. The acquisition settings used in the time series were identical to those used in measuring fluorescence intensity indices, with images obtained every 2 min for the length of the movie. The resultant time-lapse stacks were assembled into a time series as z projections using the Review Multi Dimensional Data tool of MetaMorph.

Quantification of fluorescent signals. (i) Determination of the fluorescence intensity index (FM4-64, Mlc1-YFP, and Bem1-YFP). Stacked images were merged using summation, background correction was performed by batch processing, and then each image was thresholded for quantification manually. Thresholds were established by visually highlighting the region of tip-localized signal for the majority of hyphae in each image. A circular region of interest (ROI) was created around each hyphal tip in order to collect the mean integrated intensity (fluorescence intensity) and the area of the region. The width of the tip-localized signal was obtained using the line tool of MetaMorph and drawing across what was visibly the widest part of the thresholded tip signal. The fluorescence intensity, signal area, and signal width were collected using the Region Measurements tool in MetaMorph and exported to Microsoft Excel

(2003). The intensity index was calculated for each individually analyzed cell by dividing the integrated fluorescence intensity per unit area by the width of the signal, which, for tip-localized proteins, approximates the hyphal tip width: intensity index = (integrated fluorescence intensity per unit area)/(width of tip signal).

(ii) Analysis of FM4-64 uptake dynamics. The timing of dye uptake was determined by visually assessing vacuolar staining in the mixed WT and *rsr1*Δ/Δ hyphal culture at each time frame of the series. The reported times of vacuolar staining represent the 10-min staining period plus the time from the first frame of the movie until the appearance of vacuolar staining in both strains (which occurred simultaneously). For quantification of the final fluorescence intensity, the final frame of the time-lapse series (red channel) and the final still image of Nop1-GFP-expressing (WT) cells (green channel) were processed using "no neighbors" two-dimensional (2-D) deconvolution in MetaMorph. WT and *rsr1*Δ/Δ hyphae were identified, and measurements were taken using the mean integrated fluorescence intensity of a fixed rectangular region. The region was placed on an in-focus portion of the hyphal cell membrane and spanned into a portion of the intracellular space for both strains in the same field. Background fluorescence intensities were subtracted, and measurements were taken from at least one hypha per strain per movie (the final frame of the time-lapse series) for each of three experiments performed on different days.

(iii) Determination of the percentage of hyphae with tip-localized fluorescent signals. Images that were used to determine fluorescence intensity indices were also used to determine the overall percentage of hyphae displaying tip localization of polarity proteins (Mlc1 or Bem1). Hyphal tips that were in focus in DIC images were marked with the Circular ROI tool of MetaMorph and counted to determine the total number of hyphae in the analysis. The ROIs were transferred from the DIC image to the corresponding fluorescent image, and visible tip-localized signals were manually counted and reported as a percentage of the total hyphae.

FRAP. WT and *rsr1*Δ/Δ strains were grown on coverslips under hypha-inducing conditions, stained with 5 μl of 165 mM FM4-64 for 2 min, and washed prior to imaging on an inverted Olympus Fluoroview 2000 microscope (60×/1.42 UPlanApoN objective using 3× digital zoom). A fixed-size circular ROI was placed over the FM4-64-stained Spk of each hypha. Three images were collected for baseline fluorescence measurements before bleaching for 2.5 s using a 408-nm laser. Recovery images were collected at ~1 frame/s, using the streaming function, until recovery reached a plateau (30 to 40 s). Recovery intensities were normalized (31), and the resulting recovery curves were fitted using the nonlinear regression tool of SigmaPlot (version 10.0; Systat Software, San Jose, CA). The time to half-maximal recovery ($\tau_{1/2}$) values for GTs and mature hyphae of each strain were collected and analyzed for differences (see "Statistical methods" below).

qPCR. Strains were inoculated into yeast peptone adenine dextrose (YPAD) (20) medium and grown overnight at 30°C. Hyphal growth was induced by inoculating overnight cultures as a 1:20 dilution into YPAD plus 10% serum (prewarmed to 37°C), and cells were grown to obtain GTs and mature hyphae. Pseudohyphae were induced by inoculating overnight cultures into YAPD at pH 6.0 and growing them at 36°C (32) to time match the induction times of GTs and mature hyphae. Cell culture (1.5 ml) was harvested for RNA extraction using the MasterPure Yeast RNA Purification kit (Epicentre Biotechnologies, Madison, WI) according to the manufacturer's instructions. The isolated nucleic acids were then treated with DNase, RNA quantities were determined using a NanoDrop ND-1000 spectrophotometer (NanoDrop, Wilmington, DE), and RNA (1 μg) was converted to cDNA using the High-Capacity RNA-to-cDNA Kit (Applied Biosystems, Carlsbad, CA) according to the manufacturer's instructions. Quantitative real-time PCR (qPCR) was performed using a Roche LightCycler 480 instrument (Roche Diagnostics, Indianapolis, IN) equipped with LightCycler 480 software (release 1.5.0 SP3). Primer sequences for HSGs and actin (*ACT1*) were as previously published (3) and are reproduced in Table S2 in the supplemental material. The LightCycler 480 SYBR green I Master kit (Roche) was used to perform all qPCR experiments, and reactions were set up following the manufacturer's instructions. A total quantity of 0.025 μg of cDNA was loaded into each 20-μl reaction mixture, along with 0.25 μM each primer and 10 μl of 2× Master Mix. Samples were subjected to the following PCR program: a preincubation step of 95°C for 5 min; an amplification step of 95°C for 10 s, 60°C for 10 s, and 72°C for 10 s, repeated for 45 total cycles, with fluorescence readings taken once during the 72°C stage; and finally, a melting curve step of 95°C for 5 s, 60°C for 1 min, and a final temperature of 97°C that was achieved slowly (0.11°C/s), with fluorescence readings taken continuously. All *ACT1*-specific reactions were done in triplicate on each plate, and all HSG-specific reactions were done in duplicate on each plate. Each experiment was repeated on three separate days using newly obtained RNA from newly grown cells. Each experimental day, two identical plates that were set up together were analyzed, and each plate was run consecutively, with as little time between runs as possible. To determine the relative expression of a given HSG for a given day, the daily mean Cp (point at which sample fluorescence rises above background) for that gene was divided by the daily mean Cp for *ACT1*.

Statistical methods. (i) Choice of data set for intensity index determinations. For experiments in which the intensity index was calculated, all cells with localizable signals were counted in an effort to obtain the "truest" possible mean for each strain. However, the disparity in the numbers of cells displaying tip-localized signals left the data sets unbalanced. Thus, a random sample was selected from the original data sets using SPSS 16 (IBM, Armonk, NY). The resultant randomized sample was used in the comparative analysis if it met the following three conditions: (i) the data set contained approximately equal numbers of cells for each strain used in the experiment, (ii) approximately equal proportions of GTs and mature hyphae were represented in the data set for each strain, and (iii) a minimum of 15% of the total number of cells analyzed were represented by each date of replication across all days of the experiments.

(ii) Statistical analyses. All data analyzed statistically were repeated on at least three different days. Differences were assessed with either univariate or, when appropriate, multivariate analyses using a general linear model in SPSS 16. As part of the analysis, if the main statistical effect of the day was significant in the experimental analysis, "date" was blocked in all subsequent analyses. In cases where a blocked analysis of variance (ANOVA) was used, graphs display error bars using the standard error of the mean (SEM), and where unblocked analyses were used, the error bars represent 95% confidence intervals. Full factorial analysis of a dependent variable(s) against all fixed factors was performed initially (when appropriate), and then separate subsequent assessments for within-strain (file split by strain; fixed factor = growth stage) and between-strain (file split by growth stage; fixed factor = strain) differences were performed. When the number of comparable strains in the analysis was greater than two, *post hoc* separation-of-means procedures were performed using Tukey's honestly significant differences, or when a blocked analysis was performed, least significant differences was used.

RESULTS

Rsr1 regulators are localized to the tips of hyphae. We previously reported that Rsr1-YFP localizes to the entire cell membrane of hyphae (7) (Fig. 1A). This diffuse membrane localization, while similar to that observed in *S. cerevisiae* and in *Ashbya gossypii* (32, 33), was unexpected because strains lacking Rsr1 have defects specifically at hyphal tips. To ask if Rsr1 cycling is localized to hyphal tips, we analyzed the localization of tagged versions of the Rsr1 GTPase-activating protein (GAP), Bud2, and its guanine nucleotide exchange factor (GEF), Bud5. We looked at the localization of these proteins at the two stages of hyphal development, using the presence of the first DIC-refractive septa (when chitin was visible at septa using DIC optics) as a marker of developmental time. Cells grown under hypha-inducing conditions for short periods of

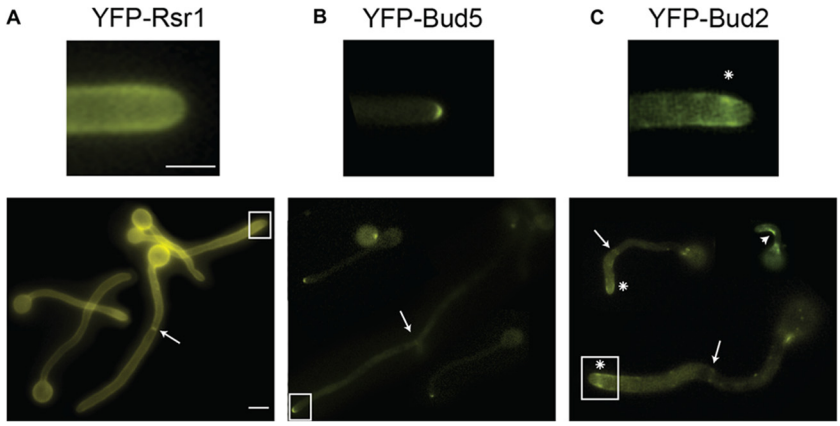

FIG 1 Positive and negative regulators of Rsr1 localize at tips of GTs and mature hyphae. Shown are representative images of strains expressing YFP-tagged versions of Rsr1 (12345) (A), Bud5 (12343) (B), and Bud2 (10055) (C). The arrows indicate enrichment of YFP-tagged proteins at septa. (C) The arrowhead denotes enrichment of YFP-Bud2 at the inner curve of a nonlinear GT; the asterisks indicate subapical enrichment of YFP-Bud2. Scale bars, 5 μm. The upper images are enlargements of the boxed areas in the lower images.

time, without septa, were deemed GTs, whereas cells grown for longer times, so that septa were present, were considered mature hyphae. YFP-Bud5 localized to the apices of GTs and mature hyphal tips in a discrete crescent (Fig. 1B) reminiscent of the polarisome proteins, Bud6 and Spa2 (12). When expressed from its native promoter, Bud2-YFP was very dim, and fairly long exposure times were needed to resolve a discrete signal. In these images, Bud2 was enriched just behind the apices of hyphal tips, appearing as a faint ring at the membrane with a relatively reduced intensity at the extreme tip (data not shown). The localization pattern was also visualized when YFP-Bud2 was expressed from the regulatable *MET3* promoter (Fig. 1C, asterisks). In addition, YFP-Bud2 was enriched in the concave angle of some curved hyphae (Fig. 1C, arrowhead) and showed discrete localization to septa (Fig. 1C, arrows), based on colocalization with Cdc12 (data not shown). The dual localization of YFP-Bud2 and YFP-Bud5 at both hyphal tips and septa suggests that their localizations during *C. albicans* hyphal morphogenesis do not vary with the cell cycle, as they do during yeast form growth (34). Thus, the localizations of the Rsr1 GAP and GEF suggest that Rsr1 activity is continuously poised to act at the tips of hyphae, where polarized growth occurs constitutively. Further, the differential localizations of Bud2 and Bud5 imply that Rsr1-GTP is enriched at the hyphal apex, whereas Rsr1-GDP is favored subapically.

The vesicular Spk is stably maintained during WT hyphal development. The presence of a Spk is associated with hyphal morphogenesis in *C. albicans* and other filamentous fungi. The vesicle component of the Spk can be visualized using FM4-64, a fluorescent lipophilic dye that is internalized by endocytosis and thereby stains the endomembrane system, which is contiguous with the Spk (12, 30). Because of its intimate association with hyphal growth, Spk integrity can be thought of as a downstream developmental characteristic of hyphal morphogenesis signaling pathways. However, because the overall appearance of the Spk varies considerably, even during WT hyphal development (Fig. 2A), we developed an intensity index (see Materials and Methods) to quantitatively describe and compare, with more accuracy and precision, Spks in WT and mutant strains with defects in polarized growth. The intensity index is a unidimensional metric akin to the morphological index described by Merson-Davies and Odds (35). It takes into account the integrated fluorescence intensity per unit area of a localized signal (here referred to simply as the fluorescence intensity) and the distribution (width) of that fluorescent signal, which approximates the hyphal-tip width. This yields a single unit that describes tip signals as a proportion of the hyphal width and facilitates the comparison of fluorescent signals in cells of different sizes. Furthermore, differences between the intensity indices of two strains can be further analyzed to determine which individual index parameter (e.g., fluorescence intensity, area, or width) contributes most to changes in the intensity index.

Between-stage analysis of FM4-64 signal characteristics at hyphal tips revealed that the intensity indices of WT Spks were the same in GTs and mature hyphae. Analysis of individual index parameters showed that Spks of mature hyphae had significantly increased fluorescence intensities compared to WT GTs ($P < 0.05$). However, the increase in intensity did not result in an increased index for mature hyphae because of a relatively small increase in the size (i.e., area and width) of the signal. Overall, the FM4-64 intensity index results indicate that despite changes in individual localization characteristics, WT Spk integrity is not different between germ tubes and mature hyphae.

Rsr1 function impacts the amount and spatial distribution of vesicles in the Spk. The morphological phenotypes of *rsr1*Δ/Δ strains indicate a defect in polarized growth (7, 8). Because the Spk is an essential organelle for polarized secretion (12), we asked if Spk characteristics differed between GTs and mature hyphae of *rsr1*Δ/Δ and WT strains. In GTs, the mean intensity index of *rsr1*Δ/Δ Spks was similar to that of WT Spks (Fig. 2B). When the individual components used to calculate the index were compared, *rsr1*Δ/Δ GTs had significantly higher vesicle intensities, areas, and widths. This indicates that although the Spks of *rsr1*Δ/Δ GTs are not identical to those of the WT, they are proportionally equal (Fig. 2B and C). In contrast, in mature hyphae, the intensity index of *rsr1*Δ/Δ Spks was significantly less than that of WT Spks. In addition, the Spk intensity index of mature *rsr1*Δ/Δ hyphae was significantly less than that of *rsr1*Δ/Δ GTs, indicating that Spk integrity is reduced over time in strains lacking Rsr1 ($P < 0.001$) (Fig. 2C). The reduced Spk intensity index of mature *rsr1*Δ/Δ hyphae was due to a decrease in intensity without a corresponding decrease in width or area of the signal. Importantly, loss of Spk

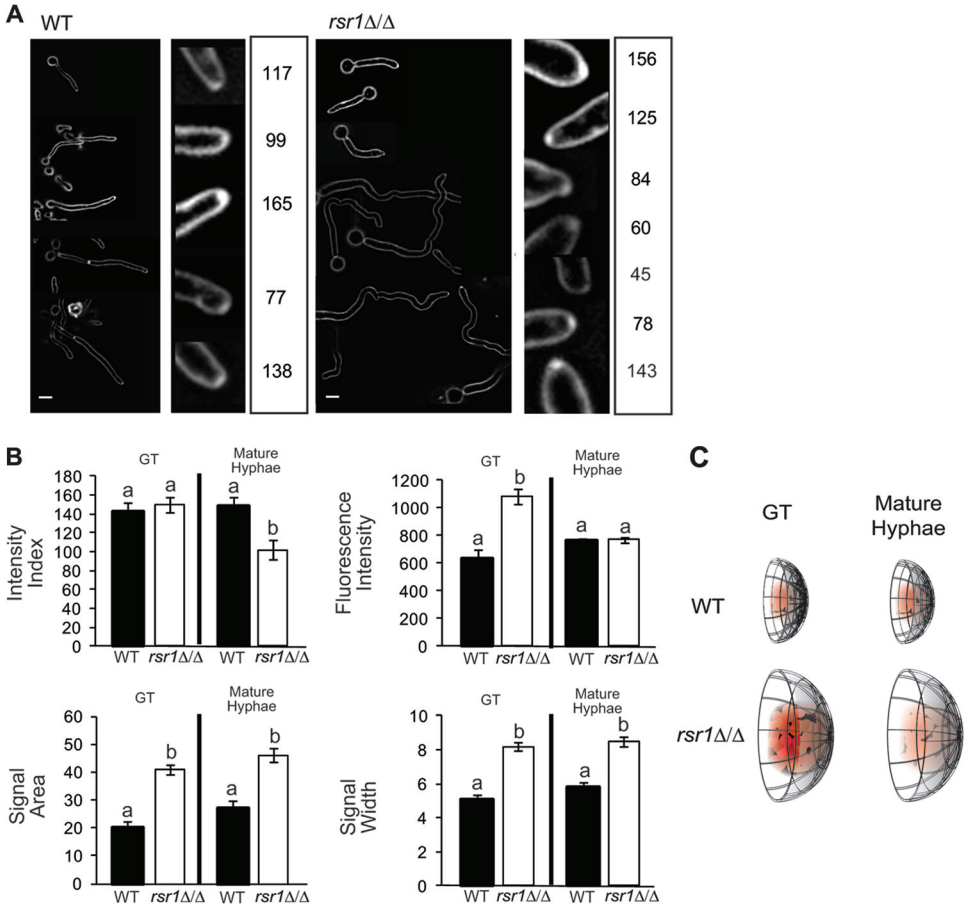

FIG 2 Comparison of vesicular Spks in WT and *rsr1*Δ/Δ hyphae. (A) Representative fluorescence images of WT (9955) and *rsr1*Δ/Δ (8880) hyphae stained with FM4-64. At the right of each set of images is the calculated intensity index for each of the representative FM4-64-stained Spks. Tip signals that appear less intense (lower fluorescence intensity) or have broader distributions (increased area and width) have lower intensity indices than signals that are more intense and/or are more focused at the hyphal tip. Scale bar, 5 μm. (B) Bar graphs depicting the mean intensity index, fluorescence intensity, area, and width of the FM4-64 signals obtained for GTs and mature hyphae of the strains shown in panel A. Stage-specific differences between strains (i.e., WT GT versus *rsr1*Δ/Δ GT, etc.) are shown. Pertinent within-strain differences between time points (i.e., WT GT versus WT mature hyphae, etc.) are stated in the text. The error bars show SEM, and data sharing the same letter (a or b) designations are not significantly different from each other. Statistical differences are at the level of a *P* value of <0.05 for both hyphal stages (~100 cells per strain for each of 3 independent experiments). (C) Diagrammatic representation of the differences in appearance of FM4-64-stained Spks of WT and *rsr1*Δ/Δ hyphae based on the data presented in panel B.

integrity was also observed when we compared *RSR1*-expressing and nonexpressing control strains (see Fig. S1 in the supplemental material), indicating that Spk phenotypes in the *rsr1*Δ/Δ strain were due to deletion of *RSR1* and not to nonspecific mutations introduced during strain construction.

The observation that overall Spk intensities and intensity indices were lower in mature *rsr1*Δ/Δ hyphae raised the possibility that vesicle delivery to hyphal tips diminishes over time in the *rsr1*Δ/Δ strain. To assess differences in vesicle delivery between GTs and mature stages of hyphal growth within each strain, FM4-64-stained membranes at the tips of WT and *rsr1*Δ/Δ hyphae were studied using FRAP (see Table S2 in the supplemental material). A significant decrease in recovery rates was observed between *rsr1*Δ/Δ GTs and mature hyphae ($P = 0.032$). In contrast, no differences were observed when we compared the recovery rates of WT GTs and mature hyphae. The change in rate observed between *rsr1*Δ/Δ GTs and mature hyphae was specific to hyphal tips, since no change in recovery rate was detected between the developmental stages when regions 10 μm behind the hyphal tip were assessed (see Table S2 in the supplemental material). The change in recovery rates seen between *rsr1*Δ/Δ GTs and mature hyphae is consistent with the data from the FM4-64 index experiments that showed a significant decrease in vesicle intensity in mature *rsr1*Δ/Δ hyphae compared to *rsr1*Δ/Δ GTs ($P < 0.001$). Taken together, the results from the FM4-64 index analysis and FRAP experiments imply that Rsr1 is involved in regulating the number and spatial distribution of vesicles and their recruitment to hyphal tips. Further, the changes observed between stages of growth in *rsr1*Δ/Δ strains indicate that the requirements for Rsr1 may differ between early (GT) and mature hyphae.

FM4-64 staining of the Spk and other cellular structures requires uptake of the dye by endocytosis. To control for potential differences in dye uptake between *rsr1*Δ/Δ and WT strains, we compared them with respect to the rate of vacuolar staining and the final fluorescence intensity of FM4-64 in both GTs and mature hyphae. To eliminate differences in the timing of dye uptake due to preparation of the strains for imaging, we mixed the control WT strain marked with a nuclear GFP reporter with a nonfluores-

cent *rsr1*Δ/Δ strain and imaged FM4-64 uptake simultaneously in the two strains. The two strains internalized FM4-64 at similar rates for both GTs and mature hyphae, with vacuolar staining being visible by 40 to 50 min in all cases, which is within the range of time observed by other investigators (36). In addition, the final mean fluorescence intensity of cell membranes was not different between WT and *rsr1*Δ/Δ strains or within either strain between developmental stages (see Fig. S2 in the supplemental material). Thus, the differences in vesicle intensity seen in *rsr1*Δ/Δ hyphae are not due to differences in the abilities of WT and *rsr1*Δ/Δ strains to internalize FM4-64. Further, the data support the conclusion that Rsr1 is not important for endocytosis but, rather, for polarized vesicle trafficking to hyphal tips.

Rsr1 is important for Mlc1 localization within the Spk. The disruption of Spk vesicle integrity in mature *rsr1*Δ/Δ hyphae raised the possibility that Rsr1 is important for the focused localization of other Spk components. Colocalization of FM4-64-stained Spk vesicles with motor-associated proteins, like Mlc1 (12), indicates that vesicle delivery occurs, at least partly, via actin and myosin. We used Mlc1, fused to YFP, as a representative protein component of the Spk and compared its signal characteristics in GTs and mature hyphae of *rsr1*Δ/Δ and WT strains (Fig. 3A). In GTs, there was no difference between the strains with respect to the number of hyphal tips exhibiting discrete, Spk-localized Mlc1signals (Fig. 3B). The Mlc1 intensity index of *rsr1*Δ/Δ GTs was higher than that of WT GTs (Fig. 3C). In contrast to the results in GTs, mature *rsr1*Δ/Δ hyphae had significantly fewer tips containing localized Mlc1-YFP than the WT strain (Fig. 3B), despite both strains expressing the same amount of Mlc1-YFP (Fig. 3D). In mature *rsr1*Δ/Δ hyphae with localizable signal, the Mlc1-YFP intensity index was the same as that of mature WT hyphae (Fig. 3C). Comparing Mlc1-YFP localization characteristics of each strain between the two hyphal stages, WT strains maintained the Mlc1-YFP intensity index ($P = 0.106$), whereas *rsr1*Δ/Δ strains had reductions in this feature over time ($P < 0.001$). The Mlc1 results parallel those seen for FM4-64-stained vesicles; WT strains maintained similar vesicle amounts and distributions over time, whereas *rsr1*Δ/Δ strains showed decreased amounts and broader distributions of vesicles over time. To better understand the timing of Mlc1 signal "loss" from the hyphal tips of mature *rsr1*Δ/Δ hyphae, we analyzed Mlc1-YFP localization by time-lapse fluorescence microscopy. During WT hyphal development, Mlc1 localizes to two regions in the cell: constitutively to the Spk (in GTs and mature hyphae) and transiently to septa at the close of the cell cycle (12) (Fig. 3E; see Movie S1 in the supplemental material). In contrast, the Spk-localized Mlc1 signal in *rsr1*Δ/Δ GTs became dimmer as growth approached the mitotic phase of the cell cycle, when Mlc1-YFP also localizes to the septum (Fig. 3E; see Movie S2 in the supplemental material). In cases where Mlc1-YFP was visibly absent for a brief time (<10 min) from the tips of *rsr1*Δ/Δ hyphae, the hypha would continue to elongate (Fig. 3E; see Movie S2 in the supplemental material). When the Mlc1 Spk signal was not visible for longer periods, hyphal elongation paused until either Mlc1-YFP relocalized to the original site of growth or the time-lapse image acquisitions stopped. In addition, extended loss of Mlc1-Spk localization and pauses in elongation were also associated with an increased likelihood of relocalization of Mlc1 to new, ectopic growth sites (see Movies S3 and S4 in the supplemental material). Results showing that Rsr1 is important for maintaining the localization of Mlc1to hyphal tips were also obtained using *RSR1*-expressing and -nonexpressing control strains (see Fig. S3A and Movies S5 and S6 in the supplemental material). Of note, Mlc1-YFP intensity index values of the *RSR1*-expressing reintegrant control strain did not reach the levels seen in the WT strain ($P = 0.023$), suggesting that one copy of *RSR1* is not sufficient for complete restoration of WT Mlc1 localization characteristics in early hyphae (compare reintegrant results in Fig. S3B in the supplemental material to WT results in Fig. 3C). Nevertheless, the Mlc1 localization results for both the experimental and *RSR1*-reintegrant control strains support the idea that Rsr1 is important for the maintenance of Mlc1 localization characteristics during hyphal morphogenesis.

Together, the results of the FM4-64 and Mlc1-YFP analyses have two important implications. First, loss of Rsr1 affects the size of the fixed region to which polarity components are delivered, since, independent of the stage of hyphal growth, the distribution of Spk markers is always broader in *rsr1*Δ/Δ hyphae than in WT hyphae (Fig. 2 and 3). Second, Rsr1 appears to be involved in both limiting the delivery of polarity components at early stages of growth (GTs) and reinforcing the delivery of those components at later stages of hyphal growth. This statement is supported by data from *rsr1*Δ/Δ strains that consistently show elevated fluorescence intensities of Spk markers in GTs and an inability to maintain those elevated intensities over time, and also by FRAP data showing a tip-specific reduction in the speed of vesicle recovery in mature *rsr1*Δ/Δ hyphae compared to GTs.

Rsr1 contributes to the maintenance of HSG expression. Cells lacking Rsr1, when grown under hyphal-induction conditions, have morphologies characteristic of both pseudohyphae and hyphae. The elongation rates of *rsr1*Δ/Δ and WT hyphae are similar, but *rsr1*Δ/Δ cells exhibit pseudohyphal-like growth, with wider cells and slight constrictions at septa (Fig. 4A) (7). Consistent with this "dual" morphology, nuclear division often takes place within elongating *rsr1*Δ/Δ cells, similar to WT hyphae, but sometimes occurs across the mother-daughter neck, similar to the nuclear division pattern of pseudohyphae (T. Heisel and C. A. Gale, unpublished data). The ability of *rsr1*Δ/Δ cells to form Spks, albeit with altered localization characteristics, is also consistent with a more hyphal than pseudohyphal developmental program. To further characterize the developmental state of *rsr1*Δ/Δ cells grown under hypha-inducing conditions, we used qPCR to compare the expression of four HSGs, *ECE1*, *HGC1*, *HYR1*, and *HWP1*, in *rsr1*Δ/Δ and WT strains. HSG expression was analyzed after growth under hyphal-induction conditions for 30 min (GTs) and 4 h (mature hyphae) (Fig. 4A). We observed decreased expression of HSGs in the *rsr1*Δ/Δ strain regardless of the developmental stage of hyphal growth (both pooled HSG results [Fig. 4B] and individual HSG results [see Fig. S4 in the supplemental material]). Indeed, HSG expression in *rsr1*Δ/Δ strains at both stages of hyphal growth was more similar to that of WT pseudohyphae than to that of either WT GTs or mature hyphae (Fig. 4B). In addition, *RSR1*-expressing reintegrant control strains showed significantly increased expression of HSGs compared to the *rsr1*-null controls, demonstrating that HSG expression defects are specific to disruption of *RSR1* (see Fig. S5 in the supplemental material). Altogether, the HSG expression results indicate that Rsr1, a landmark protein, influences the induction and maintenance of HSG expression during hyphal morphogenesis.

***RSR1* genetically interacts with regulators of *CDC42* to influence hyphal morphogenesis and HSG expression.** Similar to de-

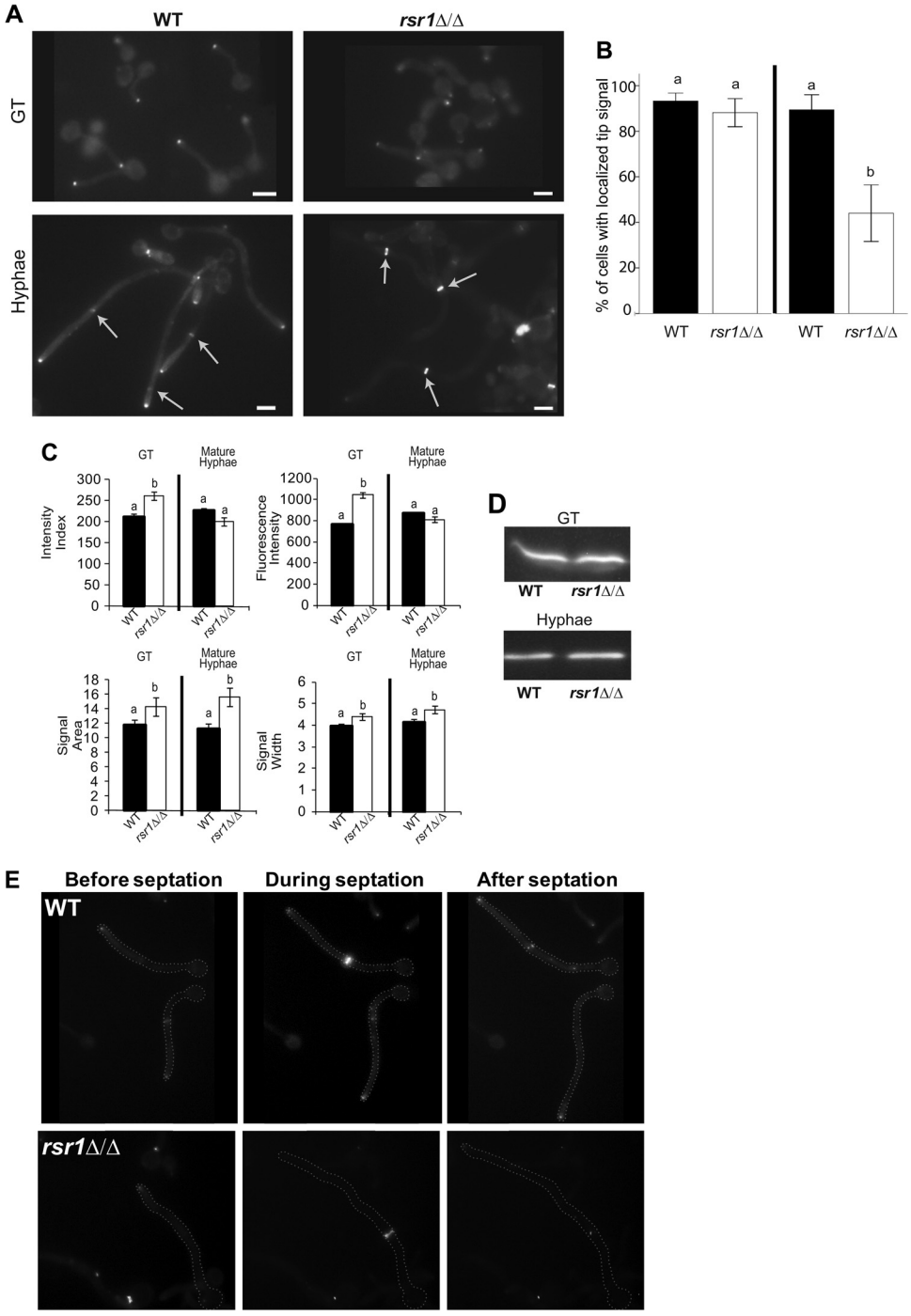

FIG 3 Comparison of Mlc1-YFP localization characteristics in WT and *rsr1*Δ/Δ hyphae. (A) Fluorescence micrographs of WT (7139) and *rsr1*Δ/Δ (11729) strains expressing Mlc1-YFP in GTs and mature hyphae. The arrows show Mlc1-YFP at septa. Scale bars, 5 μm. (B) Bar graph depicting the percentage of hyphae with localized Mlc1-YFP signal at the tip for the WT and mutant strains listed in panel A. The means represent data from an average of ~70 images for each strain from 3 independent experiments. The error bars show SEM. (C) Bar graphs depicting the mean intensity indices and index parameters of the strains shown in panel A. The means represent ~100 cells per strain from each of 3 independent experiments. Stage-specific data sharing the same letter designations are not significantly different from each other. Statistical differences are at the level of a P value of <0.05 for both hyphal stages. (D) Representative Western blot of Mlc1-YFP expression in the strains depicted in panel A at both stages of hyphal development. The mean background-subtracted ratios of Mlc1-YFP to tubulin in WT and *rsr1*Δ/Δ strains were 1.04 ± 0.18 and 1.16 ± 0.09 for GT and mature hyphae, respectively ($n = 3$). (E) Representative still fluorescence images taken from time-lapse movies (see Movies S1 and S2 in the supplemental material) of Mlc1-YFP localization in the strains shown in panel A prior to, during, and after a septation event.

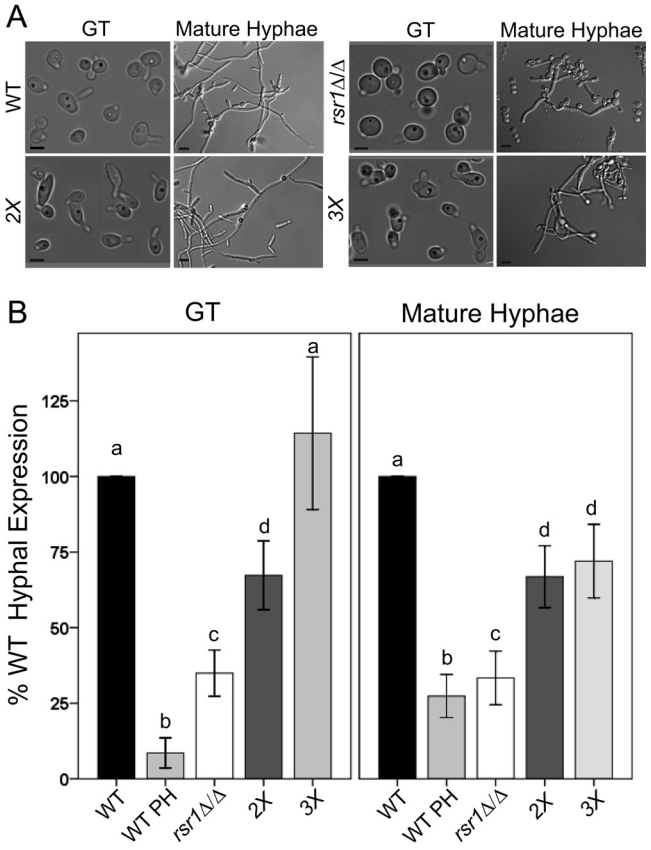

FIG 4 *RSR1* genetically interacts with *RGA2* and *BEM3*, genes that encode regulators of Cdc42, to influence the hyphal morphogenesis program. (A) Representative images of WT (9955), *rsr1*Δ/Δ (8880), *rga2*Δ/Δ *bem3*Δ/Δ (*2X*; 12188), and *rga2*Δ/Δ *bem3*Δ/Δ *rsr1*Δ/Δ (*3X*; 12191) strains. Scale bars, 5 μm in GTs, 10 μm in mature hyphae. (B) Mean pooled HSG expression levels for each strain were determined by qPCR, normalized to *ACT1* levels, and expressed as a percentage of WT HSG expression for that day ($n = 3$ for each strain). PH, pseudohyphae. Stage-specific data sharing the same letter designations are not significantly different from each other. The error bars show SEM. Statistical differences are at the level of a P value of ≤0.002 for GTs and <0.001 for mature hyphae.

letion of Rsr1, decreased expression and mutation of the essential Rho GTPase Cdc42 in *C. albicans* hyphae results in larger, rounder cells and reduced HSG expression (3–5). In *S. cerevisiae*, Rsr1 facilitates activation of Cdc42 by physically interacting with, and positioning, Cdc42 and its GEF, Cdc24 (37). To investigate the relationship between Rsr1 and Cdc42 with respect to the *C. albicans* hyphal transcriptional program, we analyzed morphology and HSG expression in an *rsr1*Δ/Δ strain that also contained deletions of the Cdc42 GAPs, Bem3 and Rga2. Deletion of Cdc42 GAPs is predicted to lower the rate of GTP hydrolysis and to result in an enrichment of membrane-associated Cdc42-GTP at hyphal tips (12). We reasoned that if the morphology and HSG expression defects of the *rsr1*Δ/Δ strain are due to reduced Cdc42 activation, then enrichment of Cdc42-GTP levels by deletion of the Cdc42 GAPs may rescue *rsr1*Δ/Δ phenotypes. Deletion of *RSR1* in combination with *RGA2* and *BEM3* (a triple-deletion strain, here referred to as the *3X* strain) resulted in narrow hyphal morphologies similar to the WT and *rga2*Δ/Δ *bem3*Δ/Δ (double-deletion, here referred to as *2X*) strains (Fig. 4A). HSG expression in the *2X* strain was reduced, however, relative to that of the WT strain, for both GTs and mature hyphae (Fig. 4B). This result suggests that while disrupting normal GTP/GDP cycling and increasing Cdc42-GTP levels affects HSG expression to a small extent, it does not dramatically affect the ability to form a WT hyphal morphology. In contrast, HSG expression in GTs of the *3X* strain did not differ from that of WT GTs and was significantly increased compared to *rsr1*Δ/Δ and *2X* GTs (Fig. 4B). HSG expression in mature *3X* hyphae was reduced to levels equal to that of the *2X* strain but still significantly higher than that of the strain containing deletion of *RSR1* alone (Fig. 4B). These HSG expression results correlate with our morphology observations (Fig. 4A). A more hypha-like morphology is seen in strains with increased HSG expression (e.g., WT, *2X*, and *3X* strains) compared to strains with lower HSG expression (e.g., the *rsr1*Δ/Δ strain). In addition, the results imply that genetic interactions between *RSR1* and regulators of *CDC42* impact HSG expression differently in GTs and mature hyphae. In GTs, loss of the Cdc42 GAPs in conjunction with deletion of *RSR1* suppresses the defects of the individual deletions. In contrast, in mature hyphae, the effect of slowing Cdc42 hydrolysis by deletion of the Cdc42 GAPs is epistatic to that of *RSR1* deletion.

Rsr1 affects the amount and distribution of Cdc42 activity at hyphal tips. To ask if the reduced HSG expression exhibited by some of the mutant strains was associated with changes in Cdc42 expression, *CDC42* mRNA and Cdc42 protein levels were determined by qPCR and Western blotting, respectively. No differences in *CDC42* expression were found in comparing WT, *rsr1*Δ/Δ, *2X*, or *3X* deletion strains in either GTs or mature hyphae ($P = 0.211$ and $P = 0.061$, respectively, by ANOVA). *CDC42* levels also did not differ between *RSR1*-expressing and -nonexpressing reintegrant control strains (data not shown). In addition, no differences were observed in Cdc42 protein levels among the strains at either time point (Fig. 5A). Thus, deletion of *RSR1* does not affect total cellular *CDC42* or Cdc42 protein levels in GTs or mature hyphae.

Although the total cellular amounts of *CDC42* and Cdc42 are not affected in hyphae lacking Rsr1, the possibility remained that Rsr1 could affect the amount and/or activity of Cdc42 specifically at hyphal tips. To compare the amounts and distributions of active Cdc42 (Cdc42-GTP) in WT and *rsr1*Δ/Δ, *2X*, and *3X* deletion strains, the expression and localization characteristics of a reporter protein, Bem1, fused to YFP were analyzed (Fig. 5A and B). Bem1 is a polarity establishment scaffolding protein that binds the GTP-bound form of Cdc42 and is used as a marker of Cdc42-GTP localization (38). No differences were observed in the amounts of Bem1-YFP expressed in GTs or mature hyphae for any of the mutant strains compared to the WT strain (Fig. 5A). In comparing the localization of Bem1-YFP, the majority of GTs of all strains had a visible tip-localized fluorescent signal (~75 to 80% of cells) (Fig. 5C); however, when the Bem1-YFP signal characteristics in GTs were compared, significant differences were observed between the strains. The fluorescence intensities of Bem1-YFP were significantly increased in *2X*, *3X*, and *rsr1*Δ/Δ GTs compared to the WT strain (Fig. 5D). The results from *2X* and *3X* strains, along with those of Court and Sudbery (25), support the idea that loss of the Cdc42 GAPs results in an enrichment of active GTP-bound Cdc42. In *rsr1*Δ/Δ GTs, the increased fluorescence intensity levels of Bem1-YFP parallel the results for FM4-64-stained vesicles and Mlc1-YFP, implying a role for Rsr1 in limiting the localization of polarity factors during early hyphal (GT) growth. However, the increased intensity of Bem1-YFP in *rsr1*Δ/Δ GTs was associated

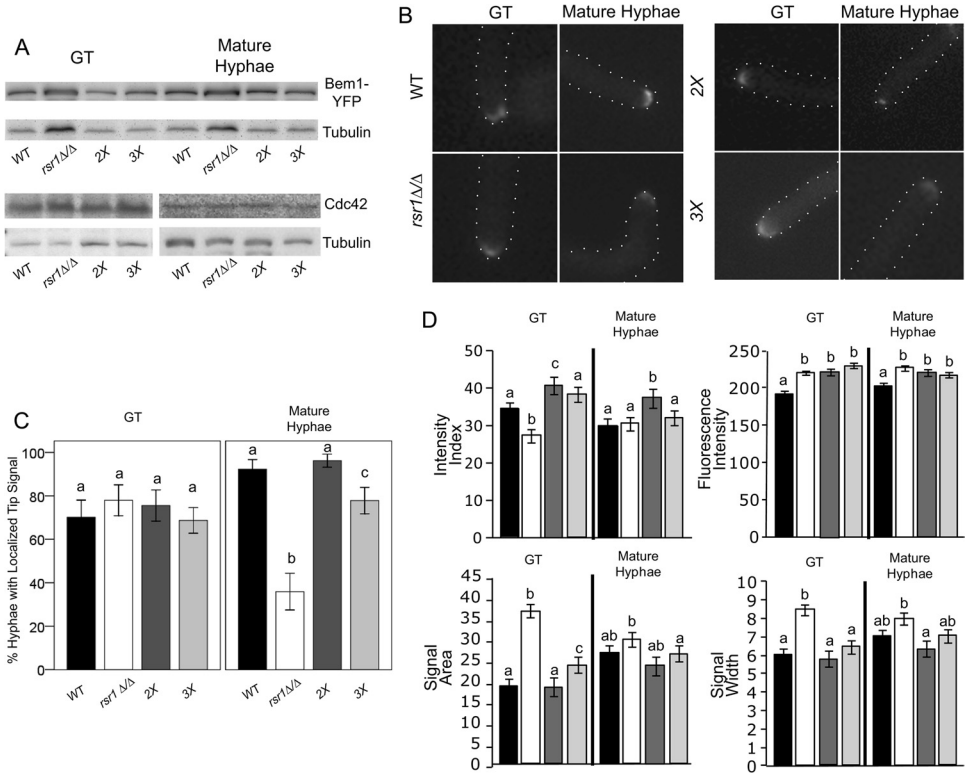

FIG 5 Rsr1 focuses Cdc42 activity at the tips of GTs and is required to maintain polarized growth in established hyphae. (A) Representative Western blot of Bem1-YFP and Cdc42 levels in GTs and mature hyphae of WT (12168) and mutant (*rsr1*Δ/Δ, 12183; *2X*, 12172; *3X*, 12173) strains. Tubulin levels are shown as a reference for protein loading. (B) Representative fluorescent images of Bem1-YFP tip localization at both stages of hyphal growth for each of the strains listed in panel A. (C) Bar graph depicting the percentages of hyphae with localized Bem1-YFP signal at the tip for the WT and mutant strains listed in panel A. The means represent data from ~60 images for each strain from 3 independent experiments. The error bars show 95% confidence intervals. (D) Bar graphs depicting the mean intensity indices and index parameters from cells with visible Bem1-YFP tip signals in GTs and mature hyphae for the strains listed in panel A. Strains are as depicted by bar shading in panel C. The means represent ~30 cells per strain from 3 independent experiments. Stage-specific data sharing the same letter designations are not significantly different from each other. Pertinent within-strain differences between time points are stated in the text. Statistical differences are at the level of a *P* value of <0.05 for both hyphal stages, and the error bars show SEM.

with a broader signal distribution, resulting in a lower, less focused Bem1-YFP intensity index than for the WT strain. In contrast, the Bem1-YFP distributions of *3X* and *2X* GTs were smaller, yielding a WT or greater-than-WT intensity index, respectively. In comparing Bem1-YFP intensity indices with HSG expression in GTs, we observed that WT Bem1-YFP intensity indices (WT and *3X* strains) are associated with WT levels of HSG induction, whereas indices that are either higher (*2X* strain) or lower (*rsr1*Δ/Δ strain) than WT are associated with reduced HSG expression.

In mature hyphae, significantly fewer *rsr1*Δ/Δ cells had visible Bem1-YFP signals at their tips than for all other strains (Fig. 5C). These results are similar to those observed in the analysis of Mlc1 localization (Fig. 3B) and are consistent with *rsr1*Δ/Δ strains being unable to maintain tip localization of polarity proteins during hyphal morphogenesis. Mature *rsr1*Δ/Δ hyphae that were able to localize Bem1-YFP to their tips exhibited an intensity index that was similar to that of mature WT hyphae ($P = 0.835$) and showed an increasing trend relative to *rsr1*Δ/Δ GTs ($P = 0.065$). Interestingly, the size (area) of the Bem1-YFP signal was the only parameter of the intensity index that showed a significant change between *rsr1*Δ/Δ GTs and mature hyphae ($P = 0.041$). This indicates that the decrease in signal area was the primary influence in mature *rsr1*Δ/Δ hyphae being able to attain a WT intensity index. The finding that some mature *rsr1*Δ/Δ hyphae do not have visible Bem1-YFP at their tips indicates that there were two potentially distinct populations of cells analyzed in the HSG expression experiments. It is possible that the population that lacked Bem1-YFP tip localization had low HSG expression levels and the population with WT Bem1-YFP localization and intensity indices had near-WT levels of HSG expression, so that together, an overall reduction in HSG expression was observed. Mature hyphae of the *2X* and *3X* strains, which were able to localize Bem1-YFP to an extent similar to that of the WT strain (Fig. 5C), exhibited more WT levels of HSG expression than mature *rsr1*Δ/Δ hyphae. In analyzing the *RSR1*-reintegrant control strain, we observed that GTs did not exhibit a WT Bem1 intensity index (see Fig. S6 in the supplemental material); however, mature hyphae did achieve WT levels for Bem1-YFP tip localization and intensity indices (see Fig. S6B and A, respectively, in the supplemental material). These data suggest that one copy of *RSR1* is not sufficient to focus Cdc42 in GTs but that one copy is sufficient to focus Cdc42 and maintain Cdc42 tip localization in mature hyphae. Altogether, the Bem1 localization results show a positive correlation between HSG expression and the focused localization of Cdc42-GTP at hyphal tips. In addition, the requirements for Rsr1 are different, depend-

ing upon the stage of hyphal growth. In GTs, Rsr1 is needed for focusing Cdc42 activity, and in mature hyphae, it is important for maintaining Cdc42 activity at hyphal tips. Further, the results are consistent with the idea that establishment of a focused distribution of Cdc42 activity in GTs is important for its continued maintenance at cell tips as hyphal development progresses.

DISCUSSION

The establishment and maintenance of polarity are highly regulated biological processes that are required for initiation of cell growth, variations in cell morphology, and generation of specialized cell types in multicellular organisms. In this study, we used a *C. albicans* strain with abnormal hyphal morphology as a tool to understand the requirements for constitutive polarized growth and the highly elongated morphology of hyphae. In *S. cerevisiae*, Rsr1 functions as a landmark, positioning new daughter cell growth with respect to that of the previous cell cycle, and is not essential for bud shape or cell size (19). Here and in previous work (7) from our laboratory, we found that deletion of the GTPase Rsr1 resulted in significant defects in polarized growth and cell shape. Similarly, in the filamentous fungus *A. gossypii*, hyphae lacking Rsr1 have defects in maintaining polarized growth and the localization of polarity structures at hyphal tips (33). Thus, in filamentous fungi, Rsr1-like proteins appear to have an expanded role in polarized growth.

The differential localization of Bud2 and Bud5 in *C. albicans* supports a role for Rsr1 activity specifically at hyphal tips. Bud5 localization predicts that the very apex of the hypha is enriched for GTP-bound Rsr1, whereas Bud2 localization predicts that GDP-bound Rsr1 is favored subapically. Given that a number of key polarity proteins (e.g., Cdc42, Cdc24, and Bem1) physically interact with the two guanine nucleotide-bound forms of Rsr1 in *S. cerevisiae* (39), a gradient of Rsr1 activity along hyphal tips could provide a way to regulate the localization and activity of Rsr1 effectors. For example, ScRsr1 has been shown to have a higher affinity for Cdc24 when Rsr1 is in its GTP-bound form, whereas the interaction between Bem1 and Rsr1 is stronger when Rsr1 is GDP bound. If this paradigm holds true in *C. albicans*, different zones of Rsr1 activity would be expected to limit the diffusion of Rsr1 effectors away from the tip and to hold them in proximity to regions of active growth.

Our results support the idea that focused localization of Cdc42 activity early in hyphal development (e.g., GTs) is related to the ability of mature hyphae to maintain polarization and the localization of polarity proteins at hyphal tips. During WT hyphal growth, Cdc42-GTP (Bem1) and its downstream targets (e.g., components of the Spk) were constitutively localized to hyphal tips and showed no significant changes in either the maintenance of their localization or focused distribution between GTs and mature hyphae. In GTs lacking Rsr1, localization of Cdc42 activity lacked focus; this was associated with an inability to maintain hyphal growth and tip localization of Bem1 and Spk components over time. Indeed, in mature *rsr1*Δ/Δ hyphae, the only cells able to maintain tip localization of Bem1 and polarized growth were those able to exhibit a WT-like focus of Cdc42 activity. The idea that mature hyphae are dependent upon processes originating in GTs is supported by the report that defects in chromatin remodeling at HSG promoters during GT growth do not affect GT morphology but yield mature hyphae with a pseudohyphal appearance and an inability to maintain expression of HSGs (40).

In *C. albicans*, we found that Rsr1 contributes to hyphal morphogenesis by regulating the amount and distribution of Cdc42 activity at hyphal tips. In addition, we observed that the ability to localize and focus Cdc42-GTP is associated with the ability to express genes specific to the hyphal transcriptional program. These results are particularly interesting, as *rsr1*Δ/Δ strains show defects in their ability to invade and cause damage in both *in vitro* and *in vivo* models of invasive candidiasis (8, 41), implying a role for tip distribution of Cdc42 in the pathogenesis process. Our results extend those of Bassilana and coworkers (3), who found that reducing the total cellular amounts of Cdc42, as well as its GEF, Cdc24, attenuated the expression of HSGs that are regulated by the transcription factor Tec1. Tec1 was also found to regulate a transient increase in Cdc24 expression at hyphal induction, suggesting that Tec1 and the Cdc42 GEF, which localizes at the hyphal tip, form a positive-feedback loop. Our data provide additional support for the idea that the tip localization and focus of Cdc42 are associated with expression of the hyphal transcriptional program. We propose that Rsr1, a landmark protein, supports this morphogenesis feedback mechanism by fine-tuning the localized distribution of Cdc42 and/or downstream targets of Cdc42 activity. It still remains to be shown how tip localization characteristics of the Cdc42 module direct gene expression. One possibility is that Cdc42 localization sets up a physical platform for actin-dependent regulation of hyphal signaling pathways. Indeed, it has been shown that *ECE1*, *HGC1*, *HWP1*, and *HYR1* are induced via the cyclic AMP (cAMP)-dependent protein kinase A signaling pathway and that their expression is reduced in the face of genetic and chemical disruptions of the actin cytoskeleton (2, 42). The recent discovery that actin and adenylate cyclase physically interact with each other in a complex and that this complex is required for the efficient production of cAMP (43) provides strong support for the idea that the cellular status of polarized actin modulates gene transcription during hyphal morphogenesis.

Overall, these results lead us to propose a model in which Rsr1 is needed to create a focused, dynamic cluster of Cdc42 activity that is associated with optimized Cdc42-dependent feedback to the hyphal transcriptional program (Fig. 6). In WT GTs, Rsr1 acts to generate a focused cluster of Cdc42 activity at hyphal tips with a limited amount of Cdc42-GTP (supported by lower Bem1 fluorescence intensities in WT than in *rsr1*Δ/Δ GTs and hyphae). In the absence of Rsr1, the clusters of Cdc42 activity that are generated contain larger amounts of Cdc42 and the localization is more broadly distributed. This results in an inability to generate the extremely narrow shape of GTs and a reduced ability to provide positive feedback to the hyphal transcriptional program. As hyphal growth progresses, if the Rsr1-independent mechanism of cluster formation is able to generate a sufficient focus of Cdc42 activity, which happens with greatly reduced efficiency, polarized growth continues (Fig. 6, pathway 2); if not, tip localization of polarity proteins is lost and the progression of polarized growth is disrupted (Fig. 6, pathway 1). Thus, elongation of GTs does not absolutely require an optimized focus of Cdc42 activity. However, if an optimal Cdc42-GTP distribution is not present by the end of the cell cycle, polarized growth will not continue. Our model is supported by results from *2X* and *3X* GTs that showed a positive relationship between increased intensity indices for Bem1-YFP and HSG expression. In GTs, the *3X* strain was the only mutant that had a WT Bem1-YFP intensity index, and this correlated with a WT HSG expression profile. This suggests that in GTs, altering

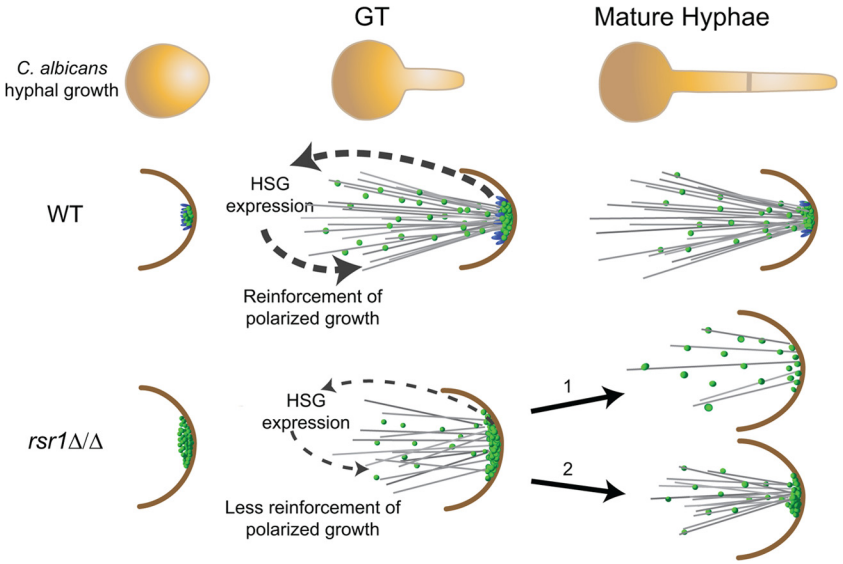

FIG 6 Model of how Rsr1 impacts the hyphal morphogenesis developmental program. In WT strains, Rsr1 (blue spheres) limits the amount of Cdc42-GTP (green spheres), focuses the distribution of Cdc42 activity during germ tube growth, and maintains the localization of Cdc42 activity during mature hyphal growth. Focused, tip-localized Cdc42 activity contributes to the induction (in GTs) and maintenance (in mature hyphae) of HSG expression, as well as maintenance of Spk integrity (not pictured). In GTs lacking Rsr1, the amount of tip-localized Cdc42-GTP is elevated relative to the WT but is also more broadly distributed at the hyphal tip. The diffuse localization of Cdc42 activity provides weak feedback and results in decreased HSG expression, as well as unregulated (excessive) delivery of Spk-associated components (not pictured) to the hyphal tip. In mature hyphae lacking Rsr1, some cells can no longer localize Cdc42 activity effectively at hyphal tips (pathway 1), whereas others in the population (i.e., those with Cdc42 distributions similar to the wild type) are able to maintain localization of Cdc42 activity, Spk integrity (not pictured), and polarized hyphal growth (pathway 2).

Cdc42 cycling in favor of the GTP-bound form compensates for the absence of Rsr1 by increasing Cdc42 focus, which in turn provides positive feedback to the hyphal program. The increase in the intensity index of the *3X* strain may have been achieved by a cytoskeleton-dependent mechanism. Given the role of active Cdc42 in directing cytoskeletal changes, holding Cdc42 in its GTP-bound state by deletion of its GAPs could have allowed sufficient reorganization of the cytoskeleton to reinforce Cdc42 activity at hyphal tips. Indeed, mathematical models of polarization events support the idea that altering Cdc42 cycling rates influences Cdc42 clustering (44). This idea is further supported by data from the *2X* strain, where altering Cdc42 cycling in the presence of the Rsr1-dependent focusing mechanism resulted in a hyperfocused Bem1 signal. Despite the higher-than-WT focus of *2X* GTs, HSG expression remained reduced compared to the WT strain. These observations suggest that, while Cdc42 enrichment drives polarized cell shapes in *C. albicans* (25), an optimized distribution of normally cycling Cdc42, mediated in part through Rsr1 activity, is required to reinforce the hyphal transcriptional program and, potentially, the expression of morphogenesis-associated virulence functions.

Although mature hyphae of the *3X* strain exhibited a WT Bem1 intensity index, they did not completely reach WT levels of HSG expression. There are two potential explanations for these findings. First, mature *3X* hyphae had a relatively small but significant loss in the number of cells exhibiting tip-localized Bem1 signal (Fig. 5). This is similar to the situation with the *rsr1*Δ/Δ strain in that the HSG data were from a mixed population of cells and thus could potentially contribute to the reduced HSG expression in the total population of mature *3X* hyphae. Alternatively, the reduced HSG expression levels of mature *3X* (and *2X*) hyphae compared to the WT strain could be attributed to changes in Cdc42-GTP hydrolysis rates. This would mean that there is an epistatic relationship between the Cdc42-GTP hydrolysis rate and the distribution of Cdc42 activity for feedback to the hyphal transcriptional program in mature hyphae. In WT strains, we propose that Rsr1 supports Cdc42 cycling so that Cdc42 activity achieves a focused distribution without a change in the rate of hydrolysis.

A "fine-tuned" amount and/or distribution of Cdc42 has been proposed to be required for cells to break symmetry and generate polarized cell shapes in the model yeast *S. cerevisiae* (16, 38). While aspects of these models are still being worked out, our results support the idea that, in *C. albicans*, Rsr1 is part of the mechanism that creates the finite window of Cdc42 activity that is needed for polarized morphogenesis of yeast, pseudohyphae, and hyphae, as well as for maintenance of continuous hyphal growth. Thus, CaRsr1 has a larger impact on polarized growth than its ortholog in *S. cerevisiae*. It is possible that an additional level of Cdc42 regulation, provided by CaRsr1, is required for the continuum of reversible morphologies exhibited by *C. albicans*. *C. albicans* and *S. cerevisiae* also differ with respect to the number of growth zones that are simultaneously present within the cell. In budding yeast, symmetry breaking is achieved by a "winning" Cdc42 cluster that initiates growth of a single bud (45, 46). In contrast, *C. albicans* hyphal development requires that Cdc42 be strongly maintained at hyphal tips, even as it transiently acts at a second site (the incipient septum) at septation (6). The observation that polarization defects took place coincident with septum formation in *rsr1*Δ/Δ hyphae implicates Rsr1 in limiting the competition for Cdc42 between the incipient septum and the hyphal tip. Similarly, recent studies in the fission yeast *Schizosaccharomyces pombe* suggest that there is a relationship between the competition for Cdc42 at multiple (bipolar) sites and polarized morphogenesis (17). Thus, we propose that the role of Rsr1 in limiting Cdc42 activity might be to serve as a mechanism that both initiates highly polarized cell

shapes and reserves a pool of Cdc42 to maintain continuous polarized growth throughout *C. albicans* hyphal development.

ACKNOWLEDGMENTS

We thank Russ Johnson, Kendra Van Beusekom, and Abigail DiPasquale for technical assistance; Maryam Gerami-Nejad and Stephen Bentivenga for technical advice; and Peter Sudbery for providing strains. We are very grateful to Judith Berman, Melissa Gardner, and the faculty of the Mount Desert Island Biological Laboratory (MDIBL) course on quantitative fluorescence microscopy for helpful discussions during preparation of the manuscript. Software support for analysis of microscopic images was provided by the Minnesota Supercomputing Institute at the University of Minnesota.

This work was supported by NIH AI057440 and University of Minnesota Pediatrics Foundation awards to C.A.G. and by an Agilent scholarship to R.P. to attend the MDIBL microscopy course.

REFERENCES

1. **Sudbery P, Gow N, Berman J.** 2004. The distinct morphogenic states of *Candida albicans*. Trends Microbiol. **12**:317–324.
2. **Johnson DI.** 1999. Cdc42: an essential Rho-type GTPase controlling eukaryotic cell polarity. Microbiol. Mol. Biol. Rev. **63**:54–105.
3. **Bassilana M, Hopkins J, Arkowitz RA.** 2005. Regulation of the Cdc42/Cdc24 GTPase module during *Candida albicans* hyphal growth. Eukaryot. Cell **4**:588–603.
4. **Ushinsky SC, Harcus D, Ash J, Dignard D, Marcil A, Morchhauser J, Thomas DY, Whiteway M, Leberer E.** 2002. *CDC42* is required for polarized growth in human pathogen *Candida albicans*. Eukaryot. Cell **1**:95–104.
5. **VandenBerg AL, Ibrahim AS, Edwards JE, Jr, Toenjes KA, Johnson DI.** 2004. Cdc42p GTPase regulates the budded-to-hyphal-form transition and expression of hypha-specific transcripts in *Candida albicans*. Eukaryot. Cell **3**:724–734.
6. **Hazan I, Liu H.** 2002. Hyphal tip-associated localization of Cdc42 is F-actin dependent in *Candida albicans*. Eukaryot. Cell **1**:856–864.
7. **Hausauer DL, Gerami-Nejad M, Kistler-Anderson C, Gale CA.** 2005. Hyphal guidance and invasive growth in *Candida albicans* require the Ras-like GTPase Rsr1p and its GTPase-activating protein Bud2p. Eukaryot. Cell **4**:1273–1286.
8. **Brand A, Vacharaksa A, Bendel C, Norton J, Haynes P, Henry-Stanley M, Wells C, Ross K, Gow NA, Gale CA.** 2008. An internal polarity landmark is important for externally induced hyphal behaviors in *Candida albicans*. Eukaryot. Cell **7**:712–720.
9. **Chaffin WL.** 1984. The relationship between yeast cell size and cell division in *Candida albicans*. Can. J. Microbiol. **30**:192–203.
10. **Herrero AB, Lopez MC, Fernandez-Lago L, Dominguez A.** 1999. *Candida albicans* and *Yarrowia lipolytica* as alternative models for analysing budding patterns and germ tube formation in dimorphic fungi. Microbiology **145**:2727–2737.
11. **Harris SD, Read ND, Roberson RW, Shaw B, Seiler S, Plamann M, Momany M.** 2005. Polarisome meets Spitzenkorper: microscopy, genetics, and genomics converge. Eukaryot. Cell **4**:225–229.
12. **Crampin H, Finley K, Gerami-Nejad M, Court H, Gale C, Berman J, Sudbery P.** 2005. *Candida albicans* hyphae have a Spitzenkorper that is distinct from the polarisome found in yeast and pseudohyphae. J. Cell Sci. **118**:2935–2947.
13. **Bartnicki-Garcia S, Bartnicki DD, Gierz G, Lopez-Franco R, Bracker CE.** 1995. Evidence that Spitzenkorper behavior determines the shape of a fungal hypha: a test of the hyphoid model. Exp. Mycol. **19**:153–159.
14. **Reynaga-Pena CG, Gierz G, Bartnicki-Garcia S.** 1997. Analysis of the role of the Spitzenkorper in fungal morphogenesis by computer simulation of apical branching in *Aspergillus niger*. Proc. Natl. Acad. Sci. U. S. A. **94**:9096–9101.
15. **Onsum MD, Rao CV.** 2009. Calling heads from tails: the role of mathematical modeling in understanding cell polarization. Curr. Opin. Cell Biol. **21**:74–81.
16. **Slaughter BD, Das A, Schwartz JW, Rubinstein B, Li R.** 2009. Dual modes of Cdc42 recycling fine-tune polarized morphogenesis. Dev. Cell **17**:823–835.
17. **Das M, Drake T, Wiley DJ, Buchwald P, Vavylonis D, Verde F.** 2012. Oscillatory dynamics of Cdc42 GTPase in the control of polarized growth. Science **337**:239–243.
18. **Irazoqui JE, Gladfelter AS, Lew DJ.** 2004. Cdc42p, GTP hydrolysis and the cell's sense of direction. Cell Cycle **3**:861–864.
19. **Bender A, Pringle JR.** 1989. Multicopy suppression of the cdc24 budding defect in yeast by *CDC42* and three newly identified genes including the ras-related gene *RSR1*. Proc. Natl. Acad. Sci. U. S. A. **86**:9976–9980.
20. **Sherman F.** 1991. Getting started with yeast. Methods Enzymol. **194**:3–20.
21. **Care RS, Trevethick J, Binley KM, Sudbery PE.** 1999. The *MET3* promoter: a new tool for *Candida albicans* molecular genetics. Mol. Microbiol. **34**:792–798.
22. **Wilson RB, Davis D, Mitchell AP.** 1999. Rapid hypothesis testing with *Candida albicans* through gene disruption with short homology regions. J. Bacteriol. **181**:1868–1874.
23. **Bensen ES, Filler SG, Berman J.** 2002. A forkhead transcription factor is important for the true hyphal as well as yeast morphogenesis in *Candida albicans*. Eukaryot. Cell **1**:787–798.
24. **Bensen ES, Clemente-Blanco A, Finley KR, Correa-Bordes J, Berman J.** 2005. The mitotic cyclins Clb2p and Clb4p affect morphogenesis in *Candida albicans*. Mol. Biol. Cell **16**:3387–3400.
25. **Court H, Sudbery P.** 2007. Regulation of Cdc42 GTPase activity in the formation of hyphae in *Candida albicans*. Mol. Biol. Cell **18**:265–281.
26. **Gerami-Nejad M, Berman J, Gale CA.** 2001. Cassettes for PCR-mediated construction of green, yellow, and cyan fluorescent protein fusions in *Candida albicans*. Yeast **18**:859–864.
27. **Gerami-Nejad M, Hausauer D, McClellan M, Berman J, Gale C.** 2004. Cassettes for the PCR-mediated construction of regulatable alleles in *Candida albicans*. Yeast **21**:429–436.
28. **Wilson RB, Davis D, Enloe BM, Mitchell AP.** 2000. A recyclable *Candida albicans URA3* cassette for PCR product-directed gene disruptions. Yeast **16**:65–70.
29. **Rasband WS.** 2004. Image J. National Institutes of Health, Bethesda, MD. http://rsb.info.nih.gov/ij.
30. **Fischer-Parton S, Parton RM, Hickey PC, Dijksterhuis J, Atkinson HA, Read ND.** 2000. Confocal microscopy of FM4-64 as a tool for analysing endocytosis and vesicle trafficking in living fungal hyphae. J. Microsc. **198**:246–259.
31. **Phair RD, Gorski SA, Misteli T.** 2004. Measurement of dynamic protein binding to chromatin in vivo, using photobleaching microscopy. Methods Enzymol. **375**:393–414.
32. **Park HO, Kang PJ, Rachfal AW.** 2002. Localization of the Rsr1/Bud1 GTPase involved in selection of a proper growth site in yeast. J. Biol. Chem. **277**:26721–26724.
33. **Bauer Y, Knechtle P, Wendland J, Helfer H, Philippsen P.** 2004. A Ras-like GTPase is involved in hyphal growth guidance in the filamentous fungus *Ashbya gossypii*. Mol. Biol. Cell **15**:4622–4632.
34. **Marston AL, Chen T, Yang MC, Belhumeur P, Chant J.** 2001. A localized GTPase exchange factor, Bud5, determines the orientation of division axes in yeast. Curr. Biol. **11**:803–807.
35. **Merson-Davies LA, Odds FC.** 1989. A morphology index for characterization of cell shape in *Candida albicans*. J. Gen. Microbiol. **135**:3143–3152.
36. **Wolf JM, Johnson DJ, Chmielewski D, Davis DA.** 2010. The *Candida albicans* ESCRT pathway makes Rim101-dependent and -independent contributions to pathogenesis. Eukaryot. Cell **9**:1203–1215.
37. **Kozminski KG, Beven L, Angerman E, Tong AH, Boone C, Park HO.** 2003. Interaction between a Ras and a Rho GTPase couples selection of a growth site to the development of cell polarity in yeast. Mol. Biol. Cell **14**:4958–4970.
38. **Kozubowski L, Saito K, Johnson JM, Howell AS, Zyla TR, Lew DJ.** 2008. Symmetry-breaking polarization driven by a Cdc42p GEF-PAK complex. Curr. Biol. **18**:1719–1726.
39. **Park HO, Bi E, Pringle JR, Herskowitz I.** 1997. Two active states of the Ras-related Bud1/Rsr1 protein bind to different effectors to determine yeast cell polarity. Proc. Natl. Acad. Sci. U. S. A. **94**:4463–4468.
40. **Lu Y, Su C, Wang A, Liu H.** 2011. Hyphal development in *Candida albicans* requires two temporally linked changes in promoter chromatin for initiation and maintenance. PLoS Biol. **9**:e1001105. doi:10.1371/journal.pbio.1001105.
41. **Falgier C, Kegley S, Podgorski H, Heisel T, Storey K, Bendel CM, Gale CA.** 2011. *Candida* species differ in their interactions with immature human gastrointestinal epithelial cells. Pediatr. Res. **69**:384–389.
42. **Wolyniak MJ, Sundstrom P.** 2007. Role of actin cytoskeletal dynamics in

activation of the cyclic AMP pathway and *HWP1* gene expression in *Candida albicans*. Eukaryot. Cell **6**:1824–1840.
43. **Zou H, Fang HM, Zhu Y, Wang Y.** 2010. *Candida albicans* Cyr1, Cap1 and G-actin form a sensor/effector apparatus for activating cAMP synthesis in hyphal growth. Mol. Microbiol. **75**:579–591.
44. **Altschuler SJ, Angenent SB, Wang Y, Wu LF.** 2008. On the spontaneous emergence of cell polarity. Nature **454**:886–889.
45. **Howell AS, Jin M, Wu CF, Zyla TR, Elston TC, Lew DJ.** 2012. Negative feedback enhances robustness in the yeast polarity establishment circuit. Cell **149**:322–333.
46. **Howell AS, Savage NS, Johnson SA, Bose I, Wagner AW, Zyla TR, Nijhout HF, Reed MC, Goryachev AB, Lew DJ.** 2009. Singularity in polarization: rewiring yeast cells to make two buds. Cell **139**:731–743.